SCIENCE CHINA
Information Sciences

• RESEARCH PAPER •

January 2024, Vol. 67, Iss. 1, 112401:1–112401:14
https://doi.org/10.1007/s11432-023-3801-1

Hybrid electromechanical properties of hetero-doped and homogeneously bonded dual-mode pressure sensor for indoor body area network node

Junbin YU[1†], Shuai XIAN[1†], Jinbiao MU[2], Min WANG[1], Yin WANG[1], Xiaojuan HOU[1], Le ZHANG[1], Jian HE[1], Jiliang MU[1*] & Xiujian CHOU[1]

[1]*Science and Technology on Electronic Test and Measurement Laboratory, North University of China, Taiyuan* 030051, *China;*
[2]*Sichuan Aerospace Fenghuo Servo Control Technology Corporation, Chengdu* 610000, *China*

Received 10 January 2023/Revised 4 April 2023/Accepted 8 June 2023/Published online 31 August 2023

Abstract Pressure sensors are considerably important for continuous monitoring of human movement and the surrounding environment to construct a caregiving system for the elderly living alone. The challenge for pressure sensors that still remains is combining self-driven, comfort, and multifunctionalization. Herein, an all-in-one conformal pressure sensor (ACPS) based on a homogeneous integrated triboelectric-piezoelectric hybrid sensor is proposed. The ACPS has dual-mode sensing properties due to coupling triboelectrification and piezoelectric effect ensuring a stable response to various external stimulations. Silver-coated glass microspheres and polyacrylonitrile were uniformly filleted into the silicone rubber substrate using a hetero-doping method to create a stretchable electrode layer with flexible conformal characteristics and a piezoelectric layer with excellent piezoelectric properties, respectively. Meanwhile, the triboelectric layer was fabricated using the same silicone rubber, allowing ACPS to be homogeneously bonded into an all-in-one structure with reliable durability. This allowed various functional layers to have outstanding interface characteristics and thus improve the electrical transmission effect. The developed ACPS had outstanding sensitivity (1.04 V/10^4 Pa), high linearity (about 0.984), a wide measurement range (10–700 kPa), and can accurately and continuously distinguish multiple movements. Furthermore, using a homemade signal processing circuit, ACPSs can be deployed in the human body and the room as indoor body area network nodes. When successfully applied to the remote tracking of daily dynamic home life and the remote operation of small electrical equipment, these ACPSs can achieve real-time caregiving for the elderly living alone. As an application area desperately needed by society, this study envisions a caregiving system for the elderly living alone without violating personal privacy.

Keywords dual-mode pressure sensor, homogeneous bonding, all-in-one structure, indoor body area network node, elderly caregiving microsystem

1 Introduction

In the past decades, the number of elderly people living alone has considerably increased [1], and their security in daily life remains an issue [2–4]. A remote monitoring system has incomparable advantages over traditional elderly care services. However, the surveillance video commonly used invades the privacy of the cared person [3, 5]. Recently, multiple sensors and portable electronic devices have been used to accurately sense the dynamic changes of moving objects and the surrounding environment [6–9]. The location coordinates and physiological data of the elderly in the room can be acquired by these sensors or electronic devices at any time, considerably improving nursing efficiency and realizing real-time monitoring of the elderly. However, traditional electronic sensors continue to rely on additional power modules such as lithium batteries and supercapacitors for power supply, which considerably reduces the

* Corresponding author (email: mujiliang@nuc.edu.cn)
† These authors contributed equally to this work.

comfort of the elderly and affects their daily life due to rigidity, service life, and environmental pollution limitations [10, 11].

The use of new generation devices, piezoelectric nanogenerators (PENGs) and triboelectric nanogenerators (TENGs), has been demonstrated to be a promising strategy for converting irregular mechanical energy into electrical energy [12–19]; meanwhile, they can also serve as self-driven physical sensors to reflect pressure changes in response to external stimuli [6, 20, 21]. The theory of hybrid nanogenerators combining these two strategies has recently been proposed to improve energy conversion efficiency resulting from the integration of different energy harvesting mechanisms [22–24], which can also sensitively detect external stimuli [25–27]. The current research in this area primarily focuses on improving the sensor output performance, and flexibility and stretchability are consistently overlooked, limiting their future applications [28, 29]. Thus, understanding how to achieve high output performance while maintaining optimal stretchability is a necessary prerequisite for the practical application of pressure sensors. The interface between electrode layers and sensitive layers of most sensors is poor due to material heterogeneity, causing device damage after multiple stretching and pressing movements [30, 31]. Furthermore, the majority of self-driven pressure sensors the are only capable of wired short-distance posture monitoring [26, 32]. There is also a part of self-driven pressure sensors that can accomplish the purpose of real-time alarm warning with the back-end circuit [28, 33], but cannot form multiple node arrays; thus, it is impossible to provide real-time, convenient, and unsupervised daily life safety monitoring for the elderly living alone.

Herein, to address these issues, we propose an all-in-one conformal pressure sensor (ACPS) that combines flexibility, stretchability, high durability, multifunctional integration, self-driven capability, and signal processing circuit assistance. Due to the combination of piezoelectric and triboelectric effects, it can realize the self-driven capability without additional power modules and improve the output performance. Meanwhile, all of the components of the ACPS are made of silicone rubber, and with the help of a multi-force mixing process and vulcanization process, electrode layers and sensitive layers can be completely integrated into an all-in-one structure with tight adhesion to ensure flexibility and stretchability, and will not be damaged even after multiple times of stretching and releasing motion, demonstrating excellent stability and durability. Based on the coupling of dual-mode sensing (piezoelectricity and triboelectricity), the ACPS exhibited outstanding sensitivity, high linearity, and fast response time when various external stimuli, such as pressing, stretching, and twisting, are present, allowing it to accurately and quickly respond to various external pressure signals to achieve sensitive perception and identification of human movement. Furthermore, ACPSs can be highly integrated with the human body and various household facilities as indoor body area network nodes, enabling remote monitoring of daily life and remote operation of household appliances using wearable technology and wireless communication technology. As a result, the novel ACPSs are placed on the elderly and in various areas of the home, and a remote tracking and control system is built by combining the self-made signal processing circuit and the upper computer to care for and facilitate the daily lives of the elderly while avoiding catastrophic events. This considerably improves the happiness, convenience, and effectiveness of family life and has broad application prospects in signal perception, medical health, and other artificial intelligence fields.

2 Experimental section

2.1 Material and fabrication

Materials. Polyacrylonitrile (PAN) powder (M_W = 1500000, M_W is molecular weight) was purchased from Hubei Dechao Chemical Co., Ltd. Silicone rubber (TNT10) and silver-coated glass microspheres (average diameter of 20–40 μm) were provided by Guangzhou Tianan Silicone Rubber Technology Co., Ltd. and Shenzhen Changxinda Shielding Material Co., Ltd., respectively. All electronic components were purchased from Shenzhen Xintong Micro Technology Co., Ltd., and all reagents were used as received.

Fabrication of ACPS. First, raw silicone and curing agent were preliminarily mixed for 30 min using a multi-force mixing process with a mass ratio of 25 : 1 to produce a blended silicone rubber (the roller rotational speed and roller spacing were finally set at 140 rad/s and 500 μm, respectively). Second, the blended silicone rubber was placed on the surface of a high-temperature-resistant sandpaper. Under high pressure, the bottom of the silicone rubber was etched on the sandpaper structure to fabricate a stretchable triboelectric layer. Subsequently, a certain quality of PAN powder was weighed and placed

into the middle of the two rollers, allowing it to be drawn into the middle of the two rollers along with the blended silicone rubber (mass ratio of PAN to silicone rubber was 3 : 5 and the roller spacing was reset to 800 μm), gradually mixing with the blended silicone rubber. At this stage, it was necessary to ensure that an appropriate amount of silicone rubber was present above the middle of the two rollers so that the PAN powder can be mixed properly. Simultaneously, the mixed silicone rubber on the top of the roller must be continuously cut for refining to help it flow and complete the mixing process for approximately 1 h. During the mixing and kneading process, the minimal spacing between the two rollers of the open mill and the difference in rotational speed between the two rollers provided strong extrusion and shear forces for the piezoelectric filler and polymer substrate, promoting uniform dispersion of the piezoelectric filler material in the substrate. At this point, the preparation of the stretchable piezoelectric layer was finished. Similarly, the silver-coated glass microspheres and blended silicone rubber were mixed in a mass ratio of 3 : 1 to create a stretchable electrode layer by the above method. After the mixing process, the layers were stacked in the order of electrode layer-piezoelectric layer-electrode layer-triboelectric layer, followed by high-temperature resistant sandpaper. Subsequently, they were placed in the center of the steel formwork (hollow structure, thickness 2.9 mm) and then in the plane vulcanizer for high temperature (175°C) and high pressure (20 MPa) vulcanization for 17 min. Figure 1(a) depicts the intuitive preparation process. Finally, the prepared sample was peeled off from the steel formwork and placed on a clean acrylic plate. The sample was cut into 3 cm × 3 cm squares with a knife and placed in the air polarization device for 1 h (polarization conditions: applied voltage of 1.60 kV and the applied temperature of 120°C). Further, the sample was cut into 2 cm × 1.8 cm pieces and used in the ACPS fabrication.

2.2 Characterization and measurement

Characterization. The morphology images of ACPSs and their corresponding composite films were obtained using a field emission scanning electron microscope (SEM, TESCAN MIRA LMS, Czech Republic). The surface elemental compositions and distribution were investigated qualitatively using an energy dispersive spectrometer (EDS, Sigma HD). The PAN was structurally and crystallographically characterized using a Rigaku Ultima IV X-ray diffractometer (XRD) with a 2θ range of 10°–50°. Fourier-transform infrared (FTIR) of the samples was performed using the Thermo Scientific Nicolet iS20 (America), and the analyzed range was between 900 to 3000 cm^{-1}.

Measurement. The ACPSs and acrylic plate (2 cm × 2 cm) were attached to the fixed and movable end of the DC linear motor, respectively. Furthermore, the DC linear motor was used to provide the magnitude and frequency of various forces, which were then used to qualitatively measure the electrical output characteristics and sensing characteristics of ACPSs. The output voltage and current of the fabricated devices were measured in real-time using an electrometer (Keithley 2611b). To achieve quantitative testing, unless otherwise noted, all devices were cut into 2 cm × 1.8 cm sizes before measuring electrical performance, and all electrical signal measurements were performed at 20 N, 1 Hz, and 600 MΩ external load resistance conditions.

3 Results and discussion

3.1 Design and characterization of the ACPS

Figure 1(a) depicts the primary fabrication process of ACPSs, and the specific preparation course is described in detail in the experiment section. Figure 1(b) depicts the conceptual diagram of the flexible/stretchable ACPS that was developed using silicone rubber, PAN powder, and silver-coated glass microspheres. Figure 1(b) clearly shows that the ACPS structure can be divided into four floors. From top to bottom, the first and third layers are stretchable electrode layers made of silicone rubber and silver-coated glass microspheres, while the second layer is a piezoelectric PAN-based composite film that forms PENG with the upper and lower electrodes. The fourth layer is pure silicone rubber with a sandpaper structure that contains ACPS as triboelectric material and forms TENG with the third layer. Thus, the ACPS integrates TENG and PENG to form a hybrid pressure sensor. Figure 1(c) depicts a physical photograph of the ACPS after the multi-force mixing and vulcanization process. It is observed that all layers of the ACPS are seamlessly combined, resulting in a complete all-in-one structure. Furthermore, to ensure ACPSs have sufficient stretchability, all parts of ACPSs were prepared on a flexible polymer

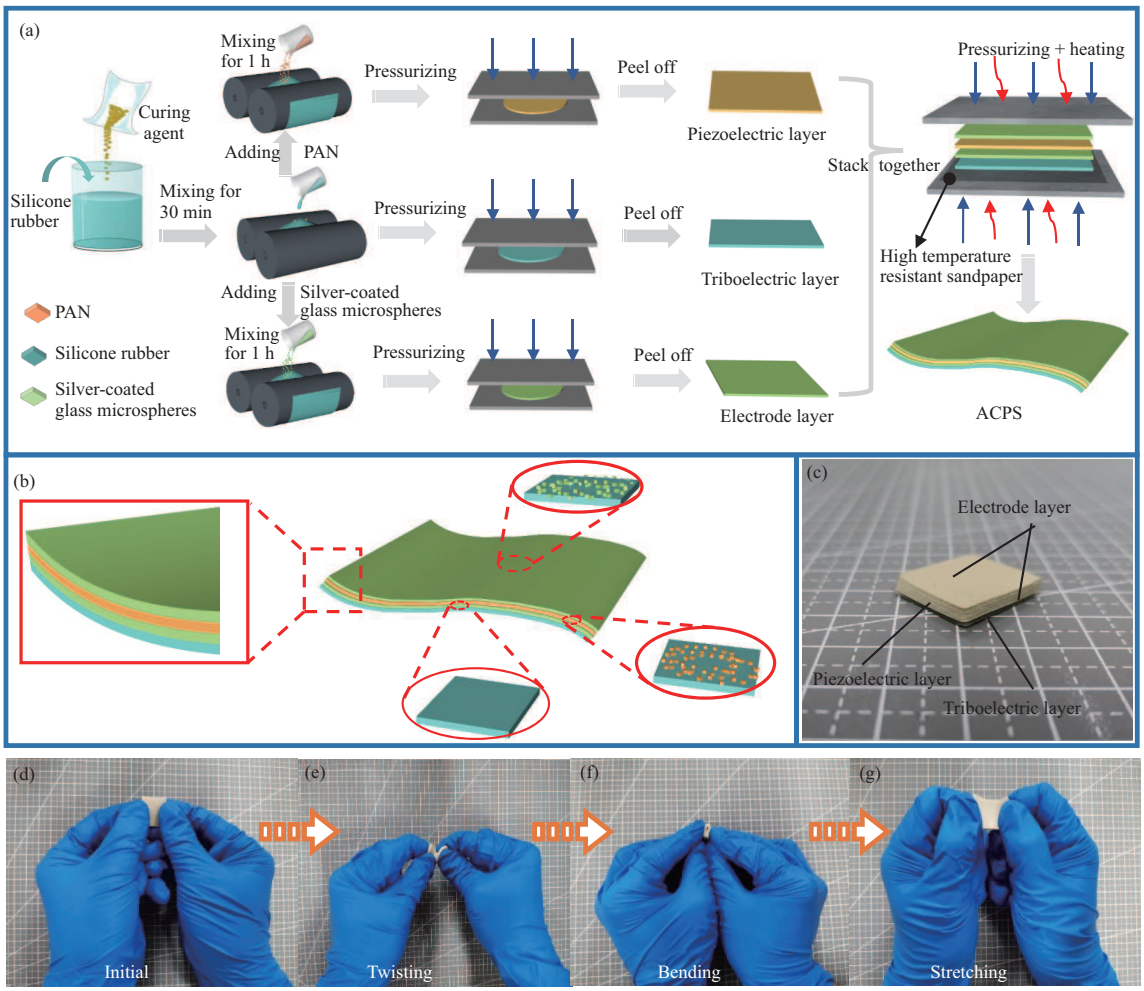

Figure 1 (Color online) Structure of the ACPS. (a) Stepwise fabrication process of the ACPS; (b) schematic and (c) digital photograph of the ACPS; (d)–(g) photographs of the ACPS in different states.

substrate. This ensured that they have outstanding flexible and stretchable properties and can be subjected to various deformation operations such as twisting, bending, and stretching (as shown in Figures 1(d)–(g)). Thus, they can be attached to any position flexibly and conveniently.

Figure 2(a) depicts an SEM image of silver-coated glass microspheres. From this figure, it can be found that their average grain diameter is around 20–40 μm. In Figure 2(b), a cross-section of the electrode layer of the ACPS with high-quality silver-coated glass microspheres evenly distributed in the silicone rubber substrate is shown. Mixing conductive fillers into flexible substrates is regarded as a good method to fabricate stretchable electrodes [34]. Figure 2(c) depicts the SEM diagram of the PAN-based composite film, revealing that PAN powder is evenly distributed in the silicone rubber substrate. Figure 2(d) depicts the surface morphology of the triboelectric layer of the ACPS. It can be observed that when compared to the film without surface modification (Figure S1(a)), there are obviously distinct irregular holes on its surface, confirming the typical sandpaper structure on the surface of the triboelectric layer. The cross-sectional view (Figure 2(e)) of the ACPS clearly shows that there is no gap between each layer, proving that it has an excellent all-in-one structure (an enlarged view of each component interface is shown in Figures S1(b) and (c)). This is because of the use of a homogeneous substrate (silicone rubber) and vulcanization process. Thus, even if ACPSs are pressed, stretched, bent, and subjected to other operations for a considerably long time, there will be no separation between the electrode layer and the sensitive layer. Figures 2(f) and (g) are EDS component analyses of the ACPS piezoelectric layer, indicating the spectral lines of Si and N elements (detailed EDS images are shown in Figure S2). Furthermore, elemental mapping displays the uniform distribution of various elements, confirming the presence of silicone rubber and PAN powder. Meanwhile, the EDS test (Ag, C, N, and Si) of the ACPS (section view) was performed and is depicted in Figure S3. Figure S3(a) shows the SEM image of the tested location, while Figure S3(b)

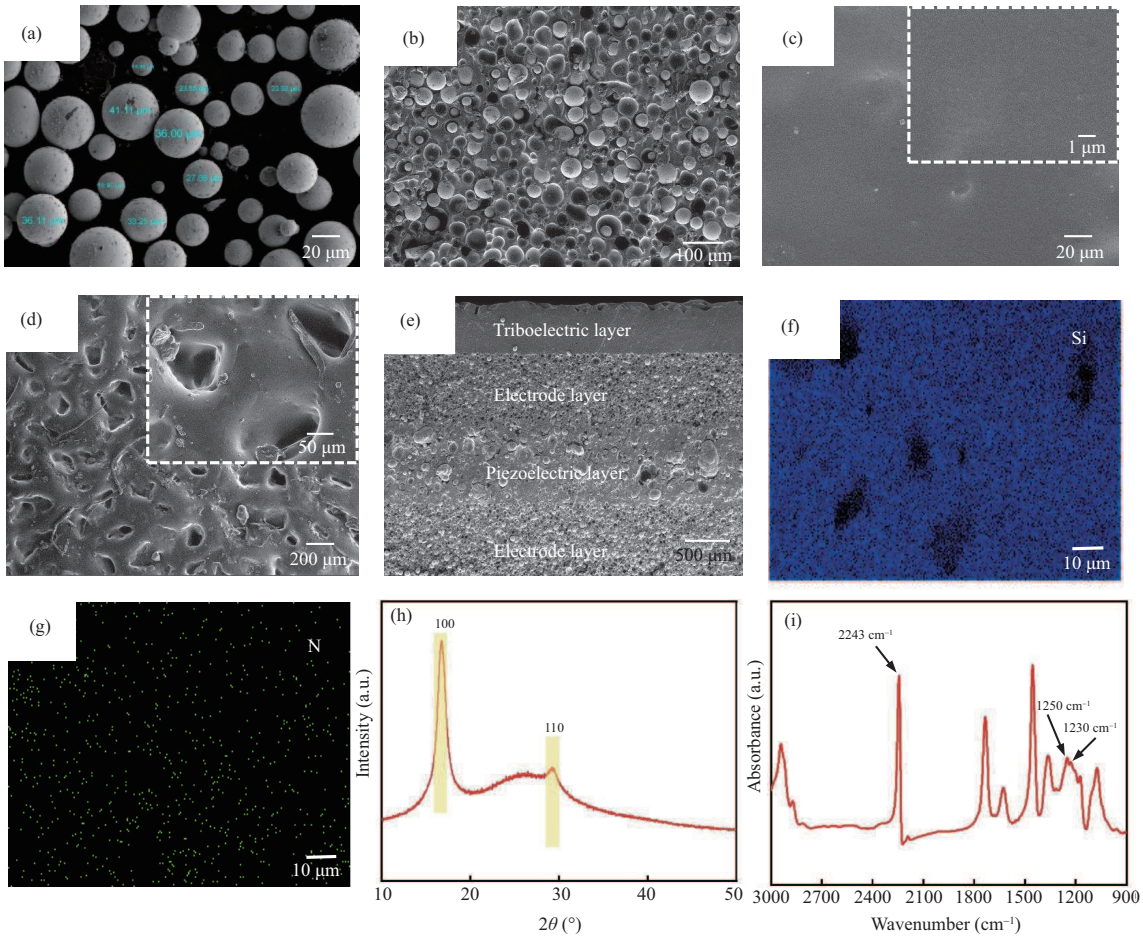

Figure 2 (Color online) Characterization of the ACPS. (a) SEM diagram of silver-coated glass microspheres; (b) SEM cross-section of the electrode layer; (c), (d) SEM images of the piezoelectric layer and triboelectric layer, respectively; (e) cross-sectional view of the ACPS; (f), (g) EDS of Si and N elements in the piezoelectric layer; (h) XRD patterns of PAN; (i) FTIR spectrum of PAN.

shows the EDS image of four elements and Figures S3(c)–(e) show the EDS images of Ag, N, and Si. Furthermore, in the solid state, PAN had planar zigzag and 3^1-helical conformations [35, 36], and the planar zigzag conformation corresponded to the better piezoelectric properties of PAN [37]. Figure 2(h) depicts the XRD pattern of PAN; the typical characteristic diffraction peak at 2θ was 17° and corresponded to the (100) crystal plane of PAN [36]. The FTIR spectrum of PAN is depicted in Figure 2(i). The absorption peak at 1230 cm^{-1} is primarily caused by the distorted vibration [$\gamma_t(CH_2)$] of the CH_2 group, representing the 3^1-helical conformation of PAN. Simultaneously, the absorption peak at 1250 cm^{-1}, which represents the planar zigzag conformation of PAN, is the result of the combined action of the plane rocking vibration [$\gamma_w(CH)$] of the CH group and the nonplane rocking vibration of the CH_2 group [35]. Furthermore, the sharp peak found at 2243 cm^{-1} is the typical absorption peak of –C≡N of PAN [38].

3.2 Working principle and electrical performance of the ACPS

The combination of PENG and TENG as a hybrid sensor ensures that the pressure sensor produces a consistent output under any condition (press or stretch). The prepared ACPS converts mechanical energy into electrical output through a combination of piezoelectric and triboelectric effects, making it more conducive to the sensing and recognition of various human posture movements. When an external object (such as human skin or silk) presses or slides on ACPSs (when the triboelectric layer contacts the object), the triboelectric charges are evenly distributed on the two surfaces, and no new triboelectric charges are generated with further pressing at the same time. At the moment, the PENG component ensures the normal operation of the sensor. When the object is in contact and separated from ACPSs, the TENG part ensures the work of the ACPS at that time. Triboelectrification, piezoelectric effect, and

electrostatic induction are the major operating mechanisms for charge accumulation and transfer in the ACPS [39]. Furthermore, in an ideal state, the piezoelectric and triboelectric parts are represented by separate circuits, and the charges generated by the two parts do not affect each other [40]. Thus, the electrical output of the ACPS can be regarded as the macroscopic sum of piezoelectric and triboelectric signals [41]. Figure 3(a) shows a schematic representation of the working principle of ACPS.

In the initial state (Figure 3(aI)), when the active layer contacts the triboelectric layer of the ACPS, the piezoelectric layer does not feel pressure. Because of the triboelectrification effect, the two materials have different adsorption capacities for electrons. The triboelectric layer has negative charges, and the surface of the active layer has an equal amount of positive charges. When the ACPS is under pressure, the piezoelectric layer deforms with external stimulation. As shown in Figures 3(aII) and (aIII), during the deformation process, the internal polarization intensity of the PAN-based composite film changes, resulting in the piezoelectric effect, which leads to the formation of piezoelectric potential. To equalize the internal polarization intensity, electrons flow from the upper electrode to the lower electrode to ensure that the upper and lower electrodes have the same amount of heterogeneous charges. When the pressure is removed, the PAN-based composite film enters a recovery state, electrons flow from the lower electrode to the upper electrode, and the piezoelectric potential decreases (Figure 3(aIV)). When the stress was removed completely, the ACPS returned to its initial state (Figure 3(aV)). Meanwhile, because the contact state between the active layer and the triboelectric layer remains constant, the triboelectric charges remain constant. Subsequently, with the further release of external stimulation, the triboelectric layer is moved far away from the active layer. To balance the potential difference caused by the electrostatic induction of the triboelectric part, electrons flow from the top electrode of the triboelectric film to the ground (Figures 3(aVI) and (aVII)). When the external stimulus is again applied to the ACPSs, the active layer becomes close to the triboelectric layer, and the electron flow direction is opposite to that shown in Figure 3(aVI), as shown in Figure 3(aVIII). With continuous external stimulation, when the object contacts the sensor again, the ACPS returns to its initial state (Figure 3(aI)), forming a complete cycle.

According to the above analysis of the working principle, it can be concluded that under continuous force, the ACPS can continuously convert mechanical energy into stable electrical output and participate in the entire working cycle due to the combination of triboelectrification and piezoelectric effect. Under the condition of reasonable connection of external circuits, Figure S4 shows the equivalent circuit model of the ACPS [41], and the electrons generated by the two components can flow in the same direction in the transition phase between triboelectrification and piezoelectric effect [42,43]. Thus, the combination of piezoelectric and triboelectric effects can effectively improve the ACPS output performance. To further confirm the preceding statement, the electrical output signals of the ACPS and its various components were further investigated, and the conductive fabric was selected as the active layer during the electrical performance test.

The single PENG part and the active layer were encapsulated with polyimide tape before testing the piezoelectric properties of the ACPS. Figures 3(b) and (e) show the voltage and current output responses of the single PENG section, respectively. Furthermore, when connected in the forward and reverse directions, the output signal is completely opposite, indicating that it is a pure piezoelectric signal [44]. According to the findings of this study, the effective area of TENG can be improved by increasing the surface roughness of the triboelectric layer and thus increasing its surface charge density. Therefore, the output performance of TENG can be improved. The output voltage and current relation of TENG in contact-separation mode can be calculated as follows [45]:

$$V = -\frac{Q}{S\varepsilon_0}\left(d_0 + x\left(t\right)\right) + \frac{\sigma x\left(t\right)}{\varepsilon_0}, \tag{1}$$

$$I = \frac{\mathrm{d}Q_{\mathrm{SC}}}{\mathrm{d}t} = \frac{S\sigma d_0}{\left(d_0 + x\left(t\right)\right)^2}\frac{\mathrm{d}x}{\mathrm{d}t} = \frac{S\sigma d_0 v\left(t\right)}{\left(d_0 + x\left(t\right)\right)^2}. \tag{2}$$

The output performance of TENG is positively proportional to the contact surface layer (S) (detailed representations of notations can be found in the Supporting information). Here, the surface of the triboelectric layer was modified using sandpaper to increase the surface contact area between the triboelectric layer and the active layer. Figures 3(c) and (f) revealed that surface modification plays an effective role in enhancing the output of triboelectricity. Additionally, when compared to a standard triboelectric layer sample, the output voltage and current of surface-modified TENG were considerably increased by 44% and 39%, respectively. Furthermore, the output performance of the ACPS was evaluated. As shown in

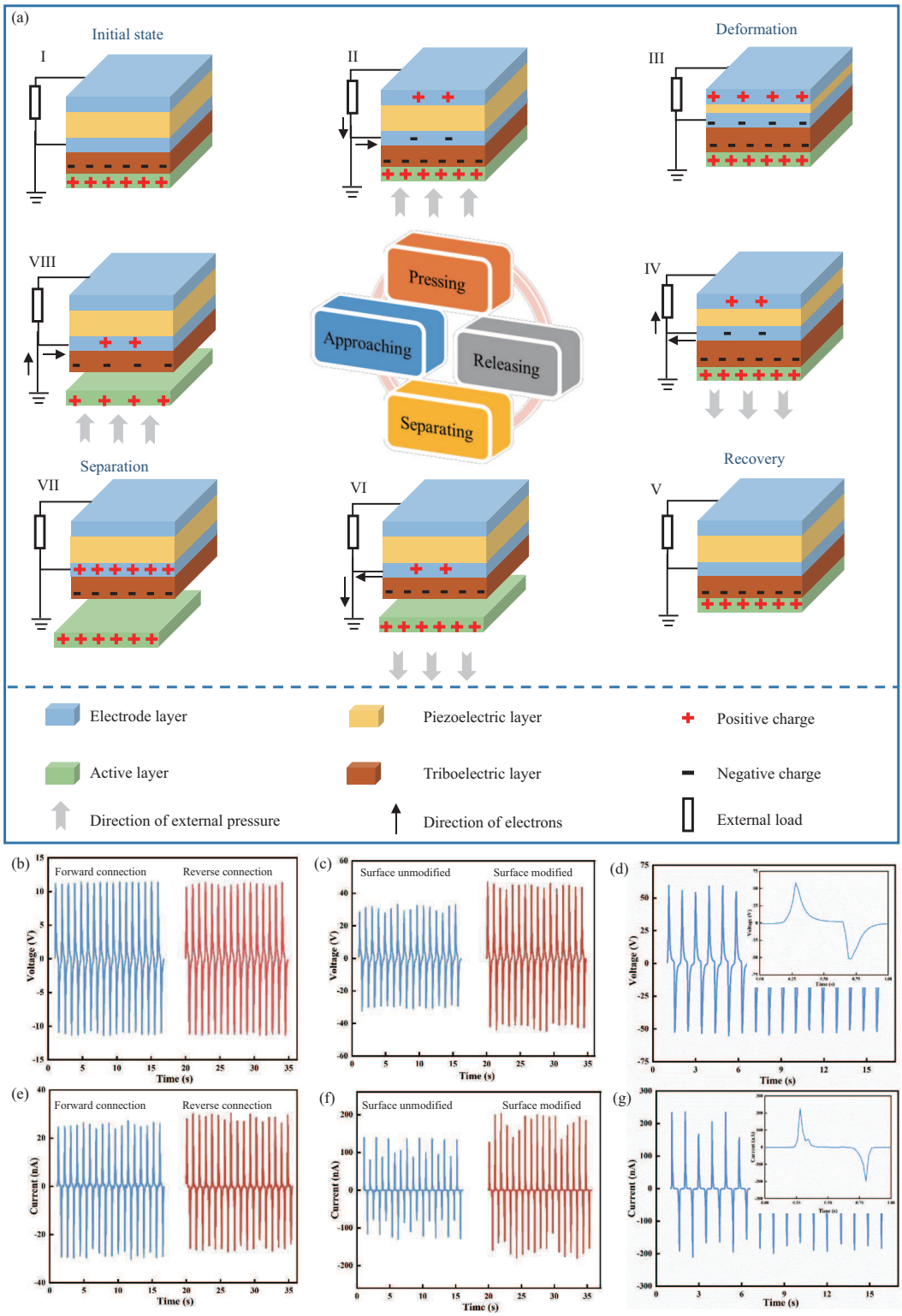

Figure 3 (Color online) (a) Working principle of the ACPS; (b)–(d) output voltage of the piezoelectric part, the triboelectric part, and the ACPS; (e)–(g) output current of the piezoelectric part, the triboelectric part, and the ACPS.

Figures 3(d) and (g), the output voltage and current of the ACPS are approximately 110 V and 410 nA, respectively, which is approximately equal to the linear superposition of PENG and TENG part outputs, and this is consistent with previous theoretical research. These theoretical and experimental results confirmed that the ACPS provides a greater output than the single PENG and TENG parts with reasonable

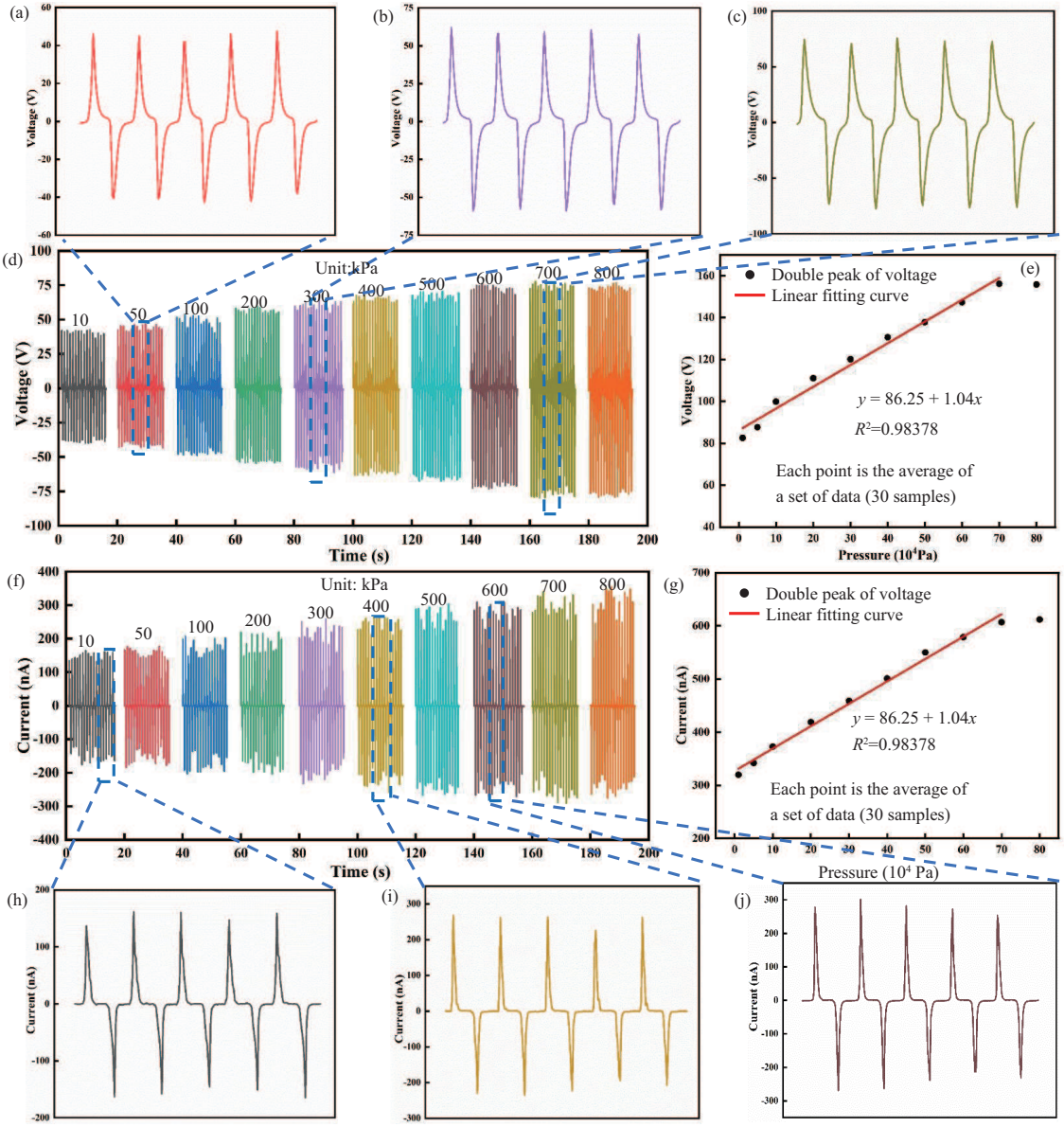

Figure 4 (Color online) Sensing characteristics of the ACPS. (a)–(c) Enlarged display diagram of some output voltage signals of the ACPS (50, 300, and 700 kPa); (d), (f) output voltage/current when the external stimulation is from 10 to 800 kPa; (e), (g) linear fitting analysis calculated from (d), (f); (h)–(j) amplified views of the output current of the ACPS at 10, 400, and 600 kPa pressure.

structural design.

Sensitivity, linearity, and detection limit are well-known key parameters for evaluating sensor performance. These parameters can directly reflect the accuracy and effect of ACPSs. The better the performance of the sensor, the greater the potential for human motion sensing and recognition, and the better it can be applied in remote tracking and control microsystems. Furthermore, when the ACPS is subjected to external force, the corresponding electrical output is produced. Thus, the effect of various pressures on the output performance of the ACPS was measured. Figures 4(d) and (f) show the output voltage and current of the ACPS when the frequency is set at 1 Hz, and the periodic linear force ranges from 10 to 800 kPa. The electric output signals of the ACPS exhibited a considerable increase from 85 to 156 V and 320 to 607 nA as the applied pressures increased from 10 to 700 kPa, and then gradually approached relative saturation at a pressure greater than 700 kPa. Additionally, to understand their changes, the five cycles of output voltage for the ACPS in periodic forces of 50, 300, and 700 kPa are depicted in Figures 4(a)–(c). Simultaneously, Figures 4(h)–(j) depict the output current of the ACPS in five complete cycles at pressures of 10, 400, and 600 kPa. The data plottings are created by averaging

the peak-to-peak value of each output signal in Figures 4(e) and (g), and the relation curves between the output of the ACPS and the magnitude of the pressures are obtained by linear fitting. In external stimulation of 10–700 kPa, the peak-to-peak voltage linear regression equation of the ACPS can be expressed using $y = 86.25 + 1.04x$, where x is the pressure on the ACPS and y is the output voltage. That is, within this range, the voltage sensitivity and linearity of the ACPS are 1.04 V/10^4 Pa (the fitting slope of the V-t curve) and 0.98373, respectively. Similarly, as shown in Figure 4(g), the current sensitivity and linearity of the ACPS are 4.21 nA/10^4 Pa and 0.99237, respectively. The ACPS can detect obvious signals at pressures as low as 10 kPa, indicating that its minimum detection limit (the threshold stress) is less than 10 kPa. Thus, the output signal of the sensor has superior linearity, outstanding sensitivity, and low detection limit, indicating that the ACPS has excellent application value.

For the pressure sensor that realizes dynamic instantaneous measurement, stability, response time, and durability are also important physical parameters to evaluate its performance. Figure 5(a) illustrates the output voltage curves of the ACPS when the external force is 20 N and the external application frequency is 1–3 Hz. It was discovered that the voltage signal of the ACPS at different frequencies is hardly affected. Previous research has shown that the output voltage of a PENG is determined by the piezoelectric modulus (d_{33}) of the piezoelectric material and the external pressure (F), regardless of the sensor's frequency. TENG's output voltage can also be calculated using (1), which is unaffected by frequency. In a nutshell, it was determined that ACPSs can still provide stable output and good stability at various frequencies. Furthermore, the response time of the sensor is determined by the time it takes for the signal to travel from baseline to peak. The faster the response speed is, the less time is required for sensing and recognition. Figure S5 depicts the ACPS response time at various frequencies while amplifying a single voltage signal. The response speed of the ACPS increases with frequency, reaching 43 ms at 3 Hz (Figure 5(d)). This implies that ACPS can react quickly to external forces and is easily distinguished. Furthermore, for daily practical applications, the ACPS's robustness and durability are also one of the most important issues. Consequently, to verify the durability of the ACPS under long-term activities and mechanical deformation, 10000 dynamic propulsion experiments were carried out. As shown in Figures 5(b) and (c), even after 10000 working cycles, the output voltage/current of the ACPS remains constant as the original and does not exhibit noticeable fluctuation or attenuation. In detail, the illustration shows the magnification images of 11 cycles extracted from data sets of 1000 and 10000 cycles. To more accurately demonstrate the stability of the ACPS in practical applications, the test cycle was extended to 20000 times to test its durability. Figure S6 shows that there is no significant difference in the output voltage/current signal between the first 500 and last 500 cycles of ACPS. All of this is due to the all-in-one structure, which prevents the ACPS output signals from degrading significantly during multiple stretching and pressing motion operations. The outcome demonstrates that good stability and robustness can be achieved in the ACPS. Furthermore, the electrical properties of the ACPS were investigated further by charging various commercial capacitors with it (see Figure S7 for charging diagram), and the results are shown in Figure 5(e). Figure 5(f) shows the details of the capacitor charging curve of 0.1 μF, and it is clear that each charging cycle of the capacitor can be seen. To summarize, the experimental results showed that the prepared ACPSs have good flexibility, stretchability, high sensitivity, a wide measurement range, a quick response time, excellent stability, and superior durability. Therefore, ACPSs can be used as self-driving and wearable pressure sensors in different application scenarios without the need for an external power supply.

3.3 ACPS-based caregiving microsystem

The aging of the population has also been deepening over the last decade, and caring for the elderly with empty nests has become a pressing social issue. Given the excellent performance of ACPSs, we created a self-driven elderly caregiving microsystem based on a smart home by placing ACPSs in different corners of the human body and indoor as indoor body area network nodes, which can not only greatly improve the nursing efficiency of the elderly, truly realize real-time monitoring of the elderly to ensure their life safety, but also significantly improve the intelligence and happiness of family life. As shown in Figure 6(a), the application system is primarily composed of a signal processing module, a wireless transmission module, an upper computer module, and some household appliances. When ACPSs embedded in the human body or furniture detect an external stimulus, they emit audible output signals. Via wireless transmission and signal processing, they can achieve remote tracking of dynamic home life and remote control of household appliances.

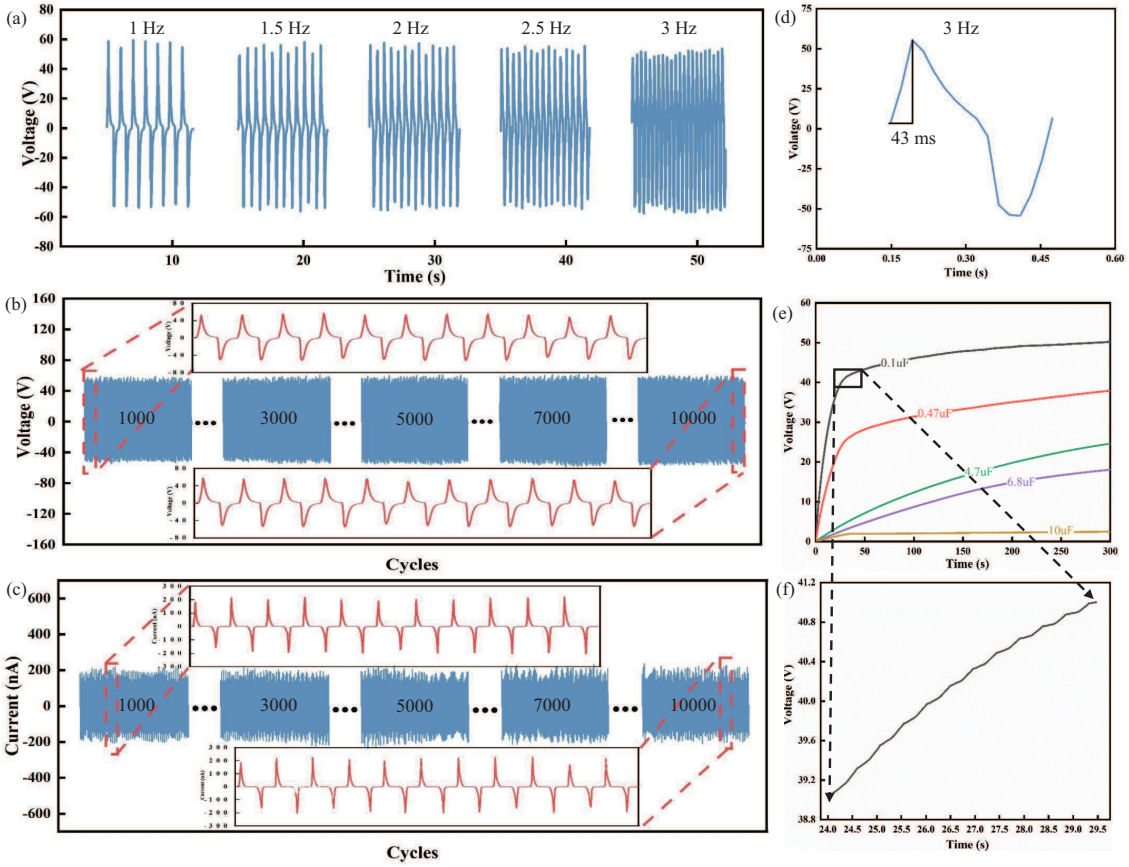

Figure 5 (Color online) (a) Frequency response of the ACPS (1–3 Hz); (b), (c) output voltage/current stability test of the ACPS; (d) response time of the ACPS under an applied pressure of 20 N at 3 Hz; (e), (f) charging curve of various capacitors (0.1, 0.47, 4.7, 6.8, and 10 μF) and the enlarged charging curve of 0.1 μF.

Figure 6(c) depicts a simple schematic diagram of a typical living room, with ACPSs placed at various joints of the human body and different positions in the living room, such as the wall, sofa, floor, and table. Furthermore, the pressure generated by human movement is typically between 100 and 370 kPa [26,46], which is entirely within the linear range of ACPSs. The flexible and stretchable ACPS was installed at the finger joint, and it can detect the movement of fingers with varying degrees of bending. Figure 6(b) and Video S1 show that when the finger is bent by 25°, 45°, and 60°, the ACPS produces different output voltages of 2.9, 5.6, and 12.6 V, respectively. As the bending angle increases, the pull-up rate of the ACPS increases, as does the amplitude of output voltage. This is because the ACPS's output signal is closely related to its force and deformation, and different finger movements can be recognized. Similarly, ACPS installed on the insole can obviously obtain output signals that differ from finger movements when the elderly walk slowly (Figure 6(d)), and the ACPS records a series of multiple signals in Figure S8 and Video S2. Hence, flexible and stretchable ACPSs have enormous potential for real-time and self-driven biomechanical sensing and recognition.

Figures 6(e)–(i) show the *V*-*t* curve when ACPSs were placed at various positions indoors and corresponding mechanical force was applied to achieve real-time tracking or persistent movement acquisition of the daily family life of the elderly living alone and in recovery training. The ACPS was placed on the chair, and based on the *V*-*t* curve of Figure 6(e), it is possible to obtain an output voltage of 101 V when people stand and sit. As shown in Figure 6(f), when the ACPS is installed in the door seam, an output voltage of about 54 V can be obtained when the door is normally opened and closed. Furthermore, as shown in Figure 6(g), when the ACPS was placed on the workbench and gently tapped with a finger, the output signal of 18 V was clearly visible (Video S3). Simultaneously, when the ACPS was integrated into the sofa's rear support (Figure 6(h) and Video S4), the voltage observed was 115 V when pressure was applied during the current period. In fact, in the indoor environment, because the scene information is relatively stable and the elderly's daily life pattern has some regularity, the waveform and amplitude of the corresponding output signal generated by stimulating ACPSs can be used as an important rep-

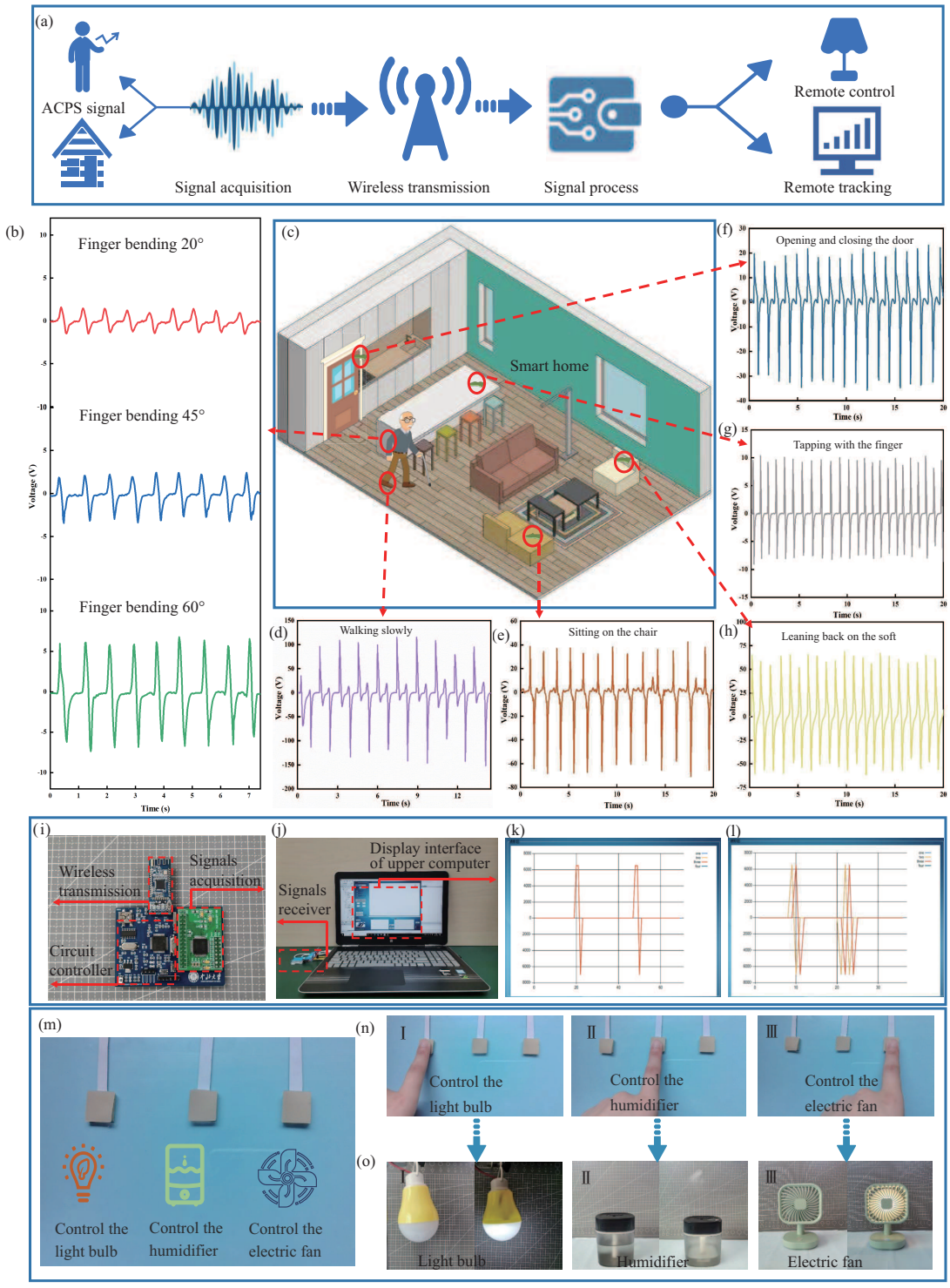

Figure 6 (Color online) (a) Schematic of the self-driven elderly caregiving microsystem based on ACPSs; (b) output voltage of the ACPS at different angles of finger bending; (c) schematic of the ACPSs deployed in various parts of a human body and a living room as body area network node; (d) output of the ACPS during the slow walking of the elderly; (e)–(h) output voltage of the ACPSs generated during various mechanical activities involved in the indoor; demonstration photograph of (i) the signal control circuit and (j) the upper computer module and receiving module of the remote tracking application; (k), (l) real-time display of remote tracking; (m) photographs of the remote small electrical equipment control panel; (n), (o) function demonstration of remote control small electrical equipment, (I) light bulb, (II) humidifier, and (III) electric fan.

resentation of the normal behavior pattern. Therefore, by developing a self-driven elderly caregiving microsystem, we can achieve remote tracking of normal indoor life dynamics. And Figures 6(i) and (j) depict the hardware circuit part (the sampling chip used in the homemade signal processing circuit is

AD7606 with a sampling rate of 200 kSPS) and the remote real-time monitoring part of the microsystem, respectively. ACPSs merged in human joints and furniture will generate electrical signals due to external pressure stimulation. These electrical signals go through signal processing, ADC (analog-to-digital converter) adjustment, and wireless transmission through the customized printed circuit board circuit board. Finally, they are received by a customized terminal display and synchronously displayed on the upper computer in real-time. To test the feasibility of indoor remote monitoring, the ACPS was installed at the human finger joint, and the electrical signal generated while the finger was bent can wirelessly transmit to the computer receiving end via the homemade circuit system for real-time remote display on the upper computer, as shown in Figure 6(k). Meanwhile, the three-channel signals yielded by multiple ACPSs integrated with each piece of furniture can be simultaneously transmitted to the upper computer for real-time display through signal processing, adjustment, and wireless transmission (Figure 6(l)).

There is one further point to mention. In addition to remote tracking the dynamic life indoors, the microsystem based on ACPSs can be extended to remote control of small electrical equipment. Multiple ACPSs are combined with a data acquisition processor, a wireless transmitter, and a receiver to create a self-driving small electrical equipment control system that controls the switches of various small electrical equipment (such as electric fans, humidifiers, and light bulbs). Figure 6(m) depicts a 3-channel ACPS array, where each sensing unit corresponds to a control command and the flexible ACPS array can be triggered by human fingers to remotely control household appliances, demonstrating the system's effectiveness and simplicity. Due to its excellent flexibility, stretchability, and stability, the ACPS array can be installed in any corner of the home or on the human body. When a human finger touched or bent the ACPSs, the corresponding sensor unit generated an electrical signal. Then, the electrical signal was processed and transmitted wirelessly via the circuit system. Finally, after receiving the switching signal, the receiver would judge and process the data again to precisely control the switch of the corresponding household appliance. Figures 6(n) and (o) and Video S5 show a comprehensive demonstration in which the first, second, and third sensing units of the ACPS array were touched to turn on the light bulb, humidifier, and electric fan, and when these sensing units were stimulated again, the corresponding small electrical equipment was turned off. Based on these features, ACPSs can be easily combined with IoT technology to easily realize remote tracking and control, providing the unparalleled advantages of traditional elderly care services for the care of the elderly living alone and in recovery training, which is conducive to improving people's lives.

4 Conclusion

Summarily, we have demonstrated a stretchable self-driven pressure sensor and proposed a new nursing method for the daily behavior of elderly people living alone. Using a simple and effective multi-force mixing process and vulcanization fabrication method, the stretchable flexible electrode was prepared to ensure that the electrode maintains excellent conductivity even when deformed. Similarly, PENG and TENG on the same substrate can achieve homogeneous bonding and are integrated into a single unit to form an all-in-one structure, and different functional layers (electrode layers, piezoelectric layer, and triboelectric layer) have good interface characteristics to improve electrical transmission effect. The dual-mode pressure sensor is built on the developed all-in-one structure by coupling piezoelectric and triboelectric effects, ensuring that ACPS can stably convert irregular mechanical energy into electrical signals under any stimulation state. The prepared ACPS has several advantages high sensitivity (1.04 V/10^4 Pa of voltage, 4.21 nA/10^4 Pa of current), a wide measurement range (10–700 kPa), good linearity (the voltage linearity is 0.98378, the current linearity is 0.99237), a fast response time (43 ms at 3 Hz), and excellent durability (over 10000 cycles). ACPS's superior electrical and sensing performance enables it to respond to various external stimulus signals accurately and quickly, as well as realize sensitive perception and recognition of human motion. Furthermore, due to ACPS's excellent flexibility, portability, and stretchability, it can be highly integrated with the human body and various household appliances. With homemade signal processing circuits, ACPSs can be successfully applied to remote monitoring of dynamic daily life and remote control of household appliances as indoor body area network nodes to achieve real-time and unsupervised caregiving for the elderly. This is critical for improving the quality of life and ensuring the safety of the elderly who live alone. This study demonstrates that ACPSs have promising application prospects in the fields of human-machine interaction, signal perception, and artificial intelligence, which will provide significant opportunities for the future development of modern

and intelligent society.

Acknowledgements This work was supported by National Natural Science Foundation of China (Grant Nos. 62101513, 62171414, 52175554, 51975542), Fundamental Research Program of Shanxi Province (Grant Nos. 201901D111146, 20210302124170), China Postdoctoral Science Foundation (Grant Nos. 2022TQ0230, 2022M712324), Shanxi "1331 Project" Key Subject Construction (Grant No. 1331KSC), and Young Academic Leaders Project of North University of China (Grant No. 11045501).

Supporting information Figures S1–S8 and Videos S1–S5. The supporting information is available online at info.scichina.com and link.springer. com. The supporting materials are published as submitted, without typesetting or editing. The responsibility for scientific accuracy and content remains entirely with the authors. The supporting information is available online at info. scichina.com and link.springer.com. The supporting materials are published as submitted, without typesetting or editing. The responsibility for scientific accuracy and content remains entirely with the authors.

References

1 Guo X, He T, Zhang Z, et al. Artificial intelligence-enabled caregiving walking stick powered by ultra-low-frequency human motion. ACS Nano, 2021, 15: 19054–19069
2 Kavuncuoğlu E, Uzunhisarcıklı E, Barshan B, et al. Investigating the performance of wearable motion sensors on recognizing falls and daily activities via machine learning. Digit Signal Process, 2022, 126: 103365
3 Zhu L H, Zhang Y, Wang Y, et al. Binocular vision positioning method for safety monitoring of solitary elderly. Comput Mater Con, 2022, 71: 593–609
4 Lin Z, Wu Z, Zhang B, et al. A triboelectric nanogenerator-based smart insole for multifunctional gait monitoring. Adv Mater Technol, 2019, 4: 1800360
5 Anaya D V, Zhan K, Tao L, et al. Contactless tracking of humans using non-contact triboelectric sensing technology: enabling new assistive applications for the elderly and the visually impaired. Nano Energy, 2021, 90: 106486
6 Zhou P, Zheng Z, Wang B, et al. Self-powered flexible piezoelectric sensors based on self-assembled 10 nm $BaTiO_3$ nanocubes on glass fiber fabric. Nano Energy, 2022, 99: 107400
7 Sun Q, Seung W, Kim B J, et al. Active matrix electronic skin strain sensor based on piezopotential-powered graphene transistors. Adv Mater, 2015, 27: 3411–3417
8 Horvitz E, Mulligan D. Data, privacy, and the greater good. Science, 2015, 349: 253–255
9 Abisegapriyan K S, Maria Joseph Raj N P, Alluri N R, et al. All in one transitional flow-based integrated self-powered catechol sensor using $BiFeO_3$ nanoparticles. Sens Actuat B-Chem, 2020, 320: 128417
10 Shi X, Luo J J, Luo J Z, et al. Flexible wood-based triboelectric self-powered smart home system. ACS Nano, 2022, 16: 3341–3350
11 Zhang T, Jiang L, Wu X Y, et al. Fingertip three-axis tactile sensor for multifingered grasping. IEEE ASME Trans Mechatron, 2015, 20: 1875–1885
12 Cao Y, Yang Y, Qu X C, et al. A self-powered triboelectric hybrid coder for human-machine interaction. Small Methods, 2022, 6: 2101529
13 Lu C F, Wu S, Zhang Y Y, et al. Electromechanical modeling of eye fatigue detecting using flexible piezoelectric sensors. Sci China Inf Sci, 2018, 61: 060417
14 Qin Y, Gao F F, Qian S, et al. Multifunctional chiral 2D lead halide perovskites with circularly polarized photoluminescence and piezoelectric energy harvesting properties. ACS Nano, 2022, 16: 3221–3230
15 Song J S, Mu J L, Li Z Y, et al. Dual-enhanced effect of ionic liquid incorporation on improving hybrid harvesting properties of solar and raindrop energy. Adv Mater Technol, 2022, 7: 2200664
16 Mu J L, He H C, Mu J B, et al. Electromechanical coupling properties of a self-powered vibration sensing device for near-surface observation tower monitoring. Sci China Tech Sci, 2022, 65: 1545–1557
17 He J, Fan X M, Zhao D Y, et al. A high-efficient triboelectric-electromagnetic hybrid nanogenerator for vibration energy harvesting and wireless monitoring. Sci China Inf Sci, 2021, 65: 142401
18 Yang Y, Luo R Z, Chao S Y, et al. Improved pharmacodynamics of epidermal growth factor via microneedles-based self-powered transcutaneous electrical stimulation. Nat Commun, 2022, 13: 6908
19 Chen Y L, Liu D, Wang S, et al. Self-powered smart active RFID tag integrated with wearable hybrid nanogenerator. Nano Energy, 2019, 64: 103911
20 Yu J B, Hou X J, He J, et al. Ultra-flexible and high-sensitive triboelectric nanogenerator as electronic skin for self-powered human physiological signal monitoring. Nano Energy, 2020, 69: 104437
21 Qu X C, Liu Z, Tan P C, et al. Artificial tactile perception smart finger for material identification based on triboelectric sensing. Sci Adv, 2022, 8: 2521
22 Wang S H, Wang Z L, Yang Y. A one-structure-based hybridized nanogenerator for scavenging mechanical and thermal energies by triboelectric-piezoelectric-pyroelectric effects. Adv Mater, 2016, 28: 2881–2887
23 Suo G Q, Yu Y H, Zhang Z Y, et al. Piezoelectric and triboelectric dual effects in mechanical-energy harvesting using $BaTiO_3$/polydimethylsiloxane composite film. ACS Appl Mater Interfaces, 2016, 8: 34335–34341
24 Deng H T, Wang Z Y, Wang Y L, et al. Integrated hybrid sensing and microenergy for compact active microsystems. Microsyst Nanoeng, 2022, 8: 61
25 Lv P P, Qian J, Yang C H, et al. Flexible all-inorganic Sm-doped PMN-PT film with ultrahigh piezoelectric coefficient for mechanical energy harvesting, motion sensing, and human-machine interaction. Nano Energy, 2022, 97: 107182
26 Yu J B, Hou X J, Cui M, et al. Highly skin-conformal wearable tactile sensor based on piezoelectric-enhanced triboelectric nanogenerator. Nano Energy, 2019, 64: 103923
27 Zou Y, Gai Y S, Tan P C, et al. Stretchable graded multichannel self-powered respiratory sensor inspired by shark gill. Fundamental Res, 2022, 2: 619–628
28 Guo Y, Zhang X S, Wang Y, et al. All-fiber hybrid piezoelectric-enhanced triboelectric nanogenerator for wearable gesture monitoring. Nano Energy, 2018, 48: 152–160
29 Wang Z, Liu Z R, Zhao G R, et al. Stretchable unsymmetrical piezoelectric $BaTiO_3$ composite hydrogel for triboelectric nanogenerators and multimodal sensors. ACS Nano, 2022, 16: 1661–1670
30 Xu F, Zhu Y. Highly conductive and stretchable silver nanowire conductors. Adv Mater, 2012, 24: 5117–5122
31 Yue X L, Xi Y, Hu C G, et al. Enhanced output-power of nanogenerator by modifying PDMS film with lateral ZnO nanotubes and Ag nanowires. RSC Adv, 2015, 5: 32566–32571

32 Shi K M, Chai B, Zou H Y, et al. Interface induced performance enhancement in flexible $BaTiO_3$/PVDF-TrFE based piezoelectric nanogenerators. Nano Energy, 2021, 80: 105515
33 Su H X, Wang X B, Li C Y, et al. Enhanced energy harvesting ability of polydimethylsiloxane-$BaTiO_3$-based flexible piezoelectric nanogenerator for tactile imitation application. Nano Energy, 2021, 83: 105809
34 Lim G H, Kwak S S, Kwon N, et al. Fully stretchable and highly durable triboelectric nanogenerators based on gold-nanosheet electrodes for self-powered human-motion detection. Nano Energy, 2017, 42: 300–306
35 Hobson R J, Windle A H. Crystalline structure of atactic polyacrylonitrile. Macromolecules, 1993, 26: 6903–6907
36 Rizzo P, Auriemma F, Guerra G, et al. Conformational disorder in the pseudohexagonal form of atactic polyacrylonitrile. Macromolecules, 1996, 29: 8852–8861
37 Sun Y, Liu Y, Zheng Y D, et al. Enhanced energy harvesting ability of ZnO/PAN hybrid piezoelectric nanogenerators. ACS Appl Mater Interfaces, 2020, 12: 54936–54945
38 Wang Q Q, Du Y Z, Feng Q, et al. Nanostructures and surface nanomechanical properties of polyacrylonitrile/graphene oxide composite nanofibers by electrospinning. J Appl Polym Sci, 2013, 128: 1152–1157
39 Wang S H, Lin L, Wang Z L. Triboelectric nanogenerators as self-powered active sensors. Nano Energy, 2015, 11: 436–462
40 Chen S, Tao X M, Zeng W, et al. Quantifying energy harvested from contact-mode hybrid nanogenerators with cascaded piezoelectric and triboelectric units. Adv Energy Mater, 2017, 7: 1601569
41 Yang J Y, Liu S D, Meng Y, et al. Self-powered tactile sensor for gesture recognition using deep learning algorithms. ACS Appl Mater Interfaces, 2022, 14: 25629–25637
42 Sun Y H, Lu Y, Li X N, et al. Flexible hybrid piezo/triboelectric energy harvester with high power density workable at elevated temperatures. J Mater Chem A, 2020, 8: 12003–12012
43 Zhu M L, Shi Q F, He T Y, et al. Self-powered and self-functional cotton sock using piezoelectric and triboelectric hybrid mechanism for healthcare and sports monitoring. ACS Nano, 2019, 13: 1940–1952
44 Yang T, Pan H, Tian G, et al. Hierarchically structured PVDF/ZnO core-shell nanofibers for self-powered physiological monitoring electronics. Nano Energy, 2020, 72: 104706
45 Niu S M, Wang S H, Lin L, et al. Theoretical study of contact-mode triboelectric nanogenerators as an effective power source. Energy Environ Sci, 2013, 6: 3576
46 Betts R P, Franks C I, Duckworth T, et al. Static and dynamic foot-pressure measurements in clinical orthopaedics. Med Biol Eng Comput, 1980, 18: 674–684